out-of-plane bending motions, are obtained with the larger 6-31G(d) and 6-31G(d,p) basis set for this planar structure.

The concerted double-hydrogen transfer transition state with D_{2h} symmetry, structure O in Figure 4, is not a true transition state on either the 6-31G(d) or 6-31G(d,p) potential energy surface. This structure has two imaginary frequencies in both basis sets. One of these frequencies corresponds to the concerted double-proton transfer, where two hydrogens move simultaneously. Following the other mode leads to the structure M, which is a minimum with C_{2v} symmetry on the 6-31G(d) potential energy surface. However, one imaginary frequency is obtained for M with the 6-31G(d,p) basis. This structure (M) lies 4.2 and 2.3 kcal/mol below O (without zero-point correction) at the SCF/6-31G(d) and SCF/6-31G(d,p) levels, respectively. The order, however, is reversed at the MP2 level of theory. MP2/6-31G(d,p)//SCF/6-31G(d) and MP2/6-31G(d,p)//SCF/6-31G(d,p) predict O to lie 3.5 and 2.5 kcal/mol below M, respectively (without zero-point correction).

The nonsymmetric transition state L with C_s symmetry has one imaginary frequency ($328i$ cm^{-1}). This is apparently the lowest energy saddle point on the SCF/6-31G(d) potential energy surface for the nonconcerted double-proton transfer in the dimer. However, a SCF/6-31G(d,p) transition-state search starting at the SCF/6-31G(d) structure L leads to structure O with C_{2v} symmetry. Energetically, the MP2/6-31G(d,p)//SCF/6-31G(d) calculation predicts structure O to be the one with the lowest overall barrier (see Table IIIC) for the dimerization-assisted double-proton transfer. This process is exothermic by 5.3 kcal/mol (without zero-point corrections) as predicted by the MP-SAC2/6-31G(d,p) method. The net energy cost for the dimer-assisted proton transfer (energy lowering due to dimer formation plus the barrier to proton transfer) is −5.3 kcal/mol.

IV. Summary and Conclusions

The present study has employed high levels of electronic structure theory to compare the [1,3] N-to-N sigmatropic rearrangement of formamidine for three mechanisms: (1) intramolecular proton transfer, (2) water-assisted double-proton transfer, and (3) dimerization-assisted double-proton transfer. All computational levels predict the barrier for (1) to be approximately twice that for (2). Energetically, the dimerization-assisted double-proton transfer appears to be the most favorable process with an enthalpy of activation of −5.8 kcal/mol followed by the water-assisted (3.5 kcal/mol) and the intramolecular (42.8 kcal/mol) processes, as predicted by MP2/6-31G(d,p). In all cases, MP-SAC2 calculations reduce the barriers, by 3–4 kcal/mol. The double-proton transfer is found to be a rather low energy process, due in large part to the energy gained by the formation of hydrogen bonds.

The water-assisted and dimerization-assisted processes are extremely sensitive to the basis sets used. To obtain reliable energetics, correlation corrections must be and were incorporated in the calculations. Polarization functions on hydrogen are also essential to locate the transition state of the dimer double-proton transfer.

We plan in future work to continue the present study by calculating rate coefficients using the present structural studies as a starting point.

Acknowledgment. This work was supported in part by the National Science Foundation (Grants CHE86-17063, CHE89-11911, and CHE89-22048) and by the Donors of the Petroleum Research Fund, administered by the American Chemical Society. These calculations were performed in part on the CRAY 1 at the Minnesota Supercomputer Institute and in part on the North Dakota State University IBM 3090 (aided by a joint study agreement with IBM) and on the NDSU Quantum Chemistry VAX 8530 (funded by a grant from the Air Force Office of Scientific Research).

Registry No. Formamidine, 463-52-5.

Crown Thioether Chemistry. The Rhodium Complexes of 1,4,7-Trithiacyclononane (9S3) and 1,5,9-Trithiacyclododecane (12S3) and the Conformational Factors That Stabilize Monomeric Rh(II) Ions

Stephen R. Cooper,* Simon C. Rawle, Rahmi Yagbasan, and David J. Watkin

Contribution from the Inorganic Chemistry Laboratory and Chemical Crystallography Laboratory, University of Oxford, Oxford OX1 3QR, England. *Received July 18, 1990*

Abstract: Reaction of the trithia ligands 9S3 (1,4,7-trithiacyclononane), 10S3 (1,4,7-trithiacyclodecane), 12S3 (1,5,9-trithiacyclododecane), and ttn (2,5,8-trithianonane) with rhodium(III) triflate in methanol yields the homoleptic thioether complexes $[Rh(L)_2]^{3+}$ (L = 9S3, 10S3, 12S3, and ttn). Average Rh–S distances in these cations increase from 2.34 Å in the 9S3 complex to 2.36 Å in the 12S3 analogue. Cyclic voltammetry in $MeNO_2$ shows that $[Rh(9S3)_2]^{3+}$ undergoes *two one-electron reductions*. The first of these corresponds to a discrete mononuclear Rh(II) complex that has been characterized by EPR as well as electrochemical methods. The 10S3 analogue, $[Rh(10S3)_2]^{3+}$, behaves similarly. In the 12S3 analogue the quasi-reversible Rh(III/II) couple contrasts with the irreversibility of the Rh(II/I) process. In continuation of this trend, the acyclic complex $[Rh(ttn)_2]^{3+}$ shows no reversible electrochemistry. The conformational properties of the macrocyclic ligand play a crucial role in stabilizing $[Rh(L)_2]^{2+}$ complexes, as shown by their increasing stability to disproportionation in the order L = 9S3 > 10S3 > 12S3 ≫ ttn. Crystal data: $[Rh(9S3)_2](CF_3SO_3)_3$, $RhC_{15}H_{24}S_9F_9O_9$, fw = 910.83, monoclinic, space group $C2/c$ (no. 15), a = 18.638 (6) Å, b = 10.643 (3) Å, c = 16.075 (2) Å, β = 105.93 (2)°, Z = 4; $[Rh(12S3)_2](BF_4)_3$, $RhC_{18}H_{36}S_6B_3F_{12}$, fw = 808.2, monoclinic, space group $P2_1/c$ (no. 14), a = 17.673 (5) Å, b = 10.874 (4) Å, c = 17.164 (3) Å, β = 110.85 (1)°, Z = 4.

Introduction

Complexes of crown thioethers such as 1,4,7-trithiacyclononane (9S3)[1] often display remarkable features (e.g., unusual stability or spin or oxidation states) that differ qualitatively from apparently analogous complexes of other thioethers.[2-4] Examples include complexes containing low-spin six-coordinate Co(II),[5] Pd(III),[6]

* To whom correspondence should be addressed.

(1) Abbreviations used: 9S3, 1,4,7-trithiacyclononane; 10S3, 1,4,8-trithiacyclodecane; 12S3, 1,5,9-trithiacyclododecane; 14S4, 1,4,8,11-tetrathiacyclotetradecane; ttn, 2,5,8-trithianonane.

0002-7863/91/1513-1600$02.50/0 © 1991 American Chemical Society

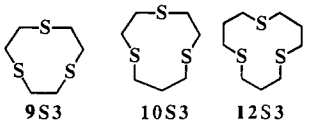

9S3 10S3 12S3

Pt(III),[7] Au(II),[8] and octahedral Ag(I).[9,10] The unusual electronic structures engendered by these ligands may induce unusual reactivity as well. Thioether complexes of rhodium attract particular interest, owing to their potential parallel to catalytically active rhodium–phosphine complexes.[11-14]

Recent investigation of 9S3 coordination chemistry led to a rare example of a monomeric Rh(II) complex.[15,16] This observation raised the question of role played by the conformational properties of 9S3, which uniquely suit it for coordination. The present investigation of $[Rh(L)_2]^{3+}$ (L = 9S3, 10S3, 12S3, and ttn), the first reported homoleptic thioether complexes of Rh(III),[17] indicates that the stability of Rh(II) in these complexes depends critically upon the conformational properties of the ligands.

Experimental Section

All solvents were freshly distilled under nitrogen from appropriate drying agents. Rhodium trichloride trihydrate (Johnson-Matthey Chemicals Ltd.) was used as supplied. Silver triflate (hemi-benzene solvate), $AgCF_3SO_3 \cdot {}^1/_2C_6H_6$, was prepared as described previously.[10] A stock solution of rhodium(III) triflate (0.08 M) was prepared by reaction of $RhCl_3 \cdot 3H_2O$ (0.53 g, 2.0 mmol) with $Ag(CF_3SO_3) \cdot {}^1/_2C_6H_6$ (1.79 mg, 6.0 mmol) in methanol (25 mL). Standard Schlenk techniques were used throughout. The synthesis of the ligands has been described previously.[18,19]

^1H NMR spectra were recorded on CD_3NO_2 solutions with a WH300 Fourier transform NMR spectrometer calibrated against residual solvent protons. Electrochemical experiments were performed under a nitrogen atmosphere on 1 mM solutions of the complexes in dry nitromethane containing 0.1 M Et_4NBF_4. A glassy carbon (GCE) working electrode was used for cyclic voltammetry, a platinum gauze for coulometry, and a saturated calomel electrode (SCE) as reference. A Princeton Applied Research Model 175 programmer, Model 179 digital coulometer, and model 173 potentiostat were used. Elemental analyses were performed by M. Gascoyne, J. Kench, and Mrs. A. Douglas of the Analytical Service of the Inorganic Chemistry Laboratory, Oxford.

Preparation of Compounds. $[Rh(9S3)_2](CF_3SO_3)_3$. A 2-mL portion (0.16 mmol) of Rh(III) triflate stock solution was refluxed overnight with 9S3 (58 mg, 0.32 mmol). On concentration and cooling, the pale orange solution deposited colorless needles (67 mg, 46%): ^1H NMR (300 MHz, CD_3NO_2) δ/ppm 3.77 (m) (cf. $[Ru(9S3)_2]^{2+}$).[20] Anal. Calcd for $RhC_{16}H_{24}S_9F_9O_9$: C, 19.78; H, 2.66. Found: C, 19.44; H, 2.58. Recrystallization from methanol gave crystals suitable for X-ray diffraction measurements.

$[Rh(10S3)_2](BF_4)_3$. A 2-mL portion (0.16 mmol) of stock Rh(III) triflate solution was refluxed overnight with 10S3 (62 mg, 0.32 mmol). After being cooled, the solution was filtered into a saturated methanolic solution of Et_4NBF_4 to precipitate the product immediately as a pale yellow powder. This was isolated by filtration, washed with a small amount of methanol, and dried in vacuo: yield 60 mg, 50%. Anal. Calcd for $C_{14}H_{28}S_6RhB_3F_{12}$: C, 22.4; H, 3.8. Found: C, 22.3; H, 3.9.

$[Rh(12S3)_2](BF_4)_3$. An identical method with use of 12S3 (71 mg, 0.32 mmol) yielded $[Rh(12S3)_2](BF_4)_3$ as a yellow powder (67 mg, 52%): ^1H NMR (300 MHz, CD_3NO_2) δ/ppm 3.42 (m) [24 H], 2.94 (m) [4 H], 2.68 (m) [4 H] (cf. $[Ru(12S3)_2]^{2+}$).[20] Anal. Calcd for $C_{18}H_{36}S_6RhB_3F_{12}$: C, 26.75; H, 4.50. Found: C, 26.79; H, 4.41. Crystals suitable for X-ray analysis were obtained by slow evaporation of a nitromethane solution.

$[Rh(ttn)_2(BF_4)_3$. A similar procedure with use of ttn (2,5,8-trithianonane, 58 mg, 0.32 mmol) yielded $[Rh(ttn)_2](BF_4)_3$ as a pale yellow powder (64 mg, 55%). Anal. Calcd for $C_{12}H_{28}S_6RhB_3F_{12}$: C, 19.79; H, 3.88. Found: C, 19.71; H, 3.90. As in the Ru(II) analogue, two methyl singlets (at δ = 2.58 and δ = 2.82 ppm) dominate the ^1H NMR spectrum (300 MHz, CD_3NO_2) and thereby indicate the unsymmetrical fac isomer.

Table I. Crystallographic Data for $[Rh(9S3)_2](CF_3SO_3)_3$ and $[Rh(12S3)_2](BF_4)_3$

	$[Rh(9S3)_2](CF_3SO_3)_3$	$[Rh(12S3)_2](BF_4)_3$
mol wt	910.83	808.16
space group	$C2/c$	$P2_1/c$
a, Å	18.638 (6)	17.673 (5)
b, Å	10.643 (3)	10.874 (4)
c, Å	16.075 (2)	17.164 (3)
α, deg	90	90
β, deg	105.93 (2)	110.85 (1)
γ, deg	90	90
vol, Å^3	3066	3083
d_{calc}, g cm^{-3}	1.97	1.74
Z	4	4
radiation	Cu Kα	Mo Kα
μ, cm^{-1}	112.14	10.18
final R, %	6.84	7.51
final R_w, %	8.65	8.83
temp	ambient	ambient
max. abs corr	2.82	1.18

Crystallography. General Procedures. In each case a crystal was sealed in a glass capillary and mounted on a CAD4 automatic diffractometer. Cu Kα radiation was used for $[Rh(9S3)_2](CF_3SO_3)_3$, while Mo Kα radiation was used for $[Rh(12S3)_2](BF_4)_3$. The unit cells and orientation matrices were determined by least-squares fitting of the setting angles of 25 reflections widely distributed in reciprocal space. Complete data sets were then collected with an ω–2θ scan. In each case, three standard reflections that were collected every hour showed no decay. Calculations were performed on a VAX 11/750 computer with the CRYSTALS[21] suite of crystallographic programs. After data reduction, during which corrections for Lorentz, polarization, and absorption effects were applied, the remaining independent reflections with $I > 3\sigma(I)$ were used for structure solution and refinement. The structures were solved by Patterson methods and refined to convergence by full-matrix least-squares techniques with anisotropic temperature factors for non-hydrogen atoms. Scattering factors were from the usual source.[22] In each case, agreement analysis indicated no systematic errors. Specific details of data collection and refinement for each structure are collected in Table I. Three term Chebyshev polynomial weighting schemes were used for both structures, with coefficients of 30.710, −16.902, and 24.667 for the Rh-9S3 structure and 12.706, −4.927, and 9.104 for the Rh-12S3 structure.

$[Rh(9S3)_2](CF_3SO_3)_3$ showed systematic absences (hkl, $h + k$ odd, $h0l$, l odd) consistent with space groups Cc or $C2/c$. Successful refinement established the latter as correct. Approximately half of the hydrogen atoms were found; all, however, were included at calculated positions, and a group isotropic thermal parameter was refined. Full-

(2) Cooper, S. R.; Rawle, S. C. *Struct. Bonding* **1990**, *72*, 1.
(3) Cooper, S. R. *Acc. Chem. Res.* **1988**, *21*, 141.
(4) Schröder, M. *Pure Appl. Chem.* **1988**, *60*, 517.
(5) Hartman, J. R.; Hintsa, E. J.; Cooper, S. R. *J. Am. Chem. Soc.* **1986**, *108*, 1208.
(6) Blake, A. J.; Holder, A. J.; Hyde, T. I.; Roberts, Y. V.; Lavery, A. J.; Schröder, M.; *J. Organomet. Chem.* **1987**, *323*, 261.
(7) Blake, A. J.; Gould, R. O.; Holder, A. J.; Hyde, T. I.; Lavery, A. J.; Odulate, M. O.; Schröder, M. *J. Chem. Soc., Chem. Commun.* **1987**, 118.
(8) Blake, A. J.; Greig, J. A.; Holder, A. J.; Hyde, T. I.; Taylor, A.; Schröder, M.; *Angew. Chem., Int. Ed. Engl.* **1990**, *29*, 197.
(9) Clarkson, J.; Yagbasan, R.; Blower, P. J.; Cooper, S. R. *J. Chem. Soc., Chem. Commun.* **1987**, 950.
(10) Blower, P. J.; Clarkson, J. A.; Rawle, S. C.; Hartman, J. R.; Wolf, R. E., Jr.; Yagbasan, R.; Bott, S. G.; Cooper, S. R., in press.
(11) Lemke, W.; Travis, K.; Takvoryan, N.; Busch, D. H. *Adv. Chem. Ser.* **1976**, *150*, 358.
(12) Yoshida, T.; Ueda, T.; Adachi, T.; Yamamoto, K.; Higuchi, T. *J. Chem. Soc. Chem. Commun.* **1985**, 1137.
(13) Travis, K.; Busch, D. H. *Inorg. Chem.* **1974**, *13*, 2591.
(14) Walton, R. A. *J. Chem. Soc. A* **1967**, 1852.
(15) Rawle, S. C.; Yagbasan, R.; Prout, K.; Cooper, S. R. *J. Am. Chem. Soc.* **1987**, *109*, 6181.
(16) Blake, A. J.; Gould, R. O.; Holder, A. J.; Hyde, T. I.; Schröder, M. *J. Chem. Soc., Dalton Trans.* **1988**, 1861.
(17) Murray, S. G.; Hartley, F. R. *Chem. Rev.* **1981**, *81*, 365.
(18) Blower, P. J.; Cooper, S. R. *Inorg. Chem.* **1987**, *26*, 2009.
(19) Wolf, R. E., Jr.; Hartman, J. R.; Ochrymowycz, L. A.; Cooper, S. R. *Inorg. Synth.* **1988**, *25*, 122.
(20) Rawle, S. C.; Sewell, T. J.; Cooper, S. R. *Inorg. Chem.* **1987**, *26*, 3769.
(21) Carruthers, J. R. CRYSTALS User Manual, Oxford University Computing Laboratory, 1975.
(22) Cromer, D. T.; Waber, J. T. *International Tables for X-ray Crystallography*; Kynoch Press: Birmingham, 1974; Vol. 4.

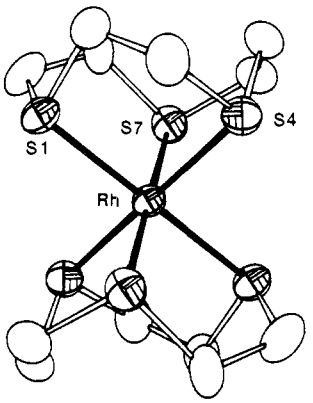

Figure 1. ORTEP diagram of $[Rh(9S3)_2]^{3+}$ (hydrogen atoms omitted for clarity). Atomic numbering follows IUPAC convention (i.e., S1, C2, C3, S3, etc.).

matrix least-squares refinement based on 1547 data with $I > 3\sigma(I)$ converged to $R = 6.84\%$ ($R_w = 8.65\%$) for 199 parameters. One of the two triflate groups' anions is disordered. Packing diagrams show that both triflate anions lie in a continuous layer. The disordered ion is at the center of a large cavity. The electron density in this region is essentially a hollow shell with broad maxima. This density can be modelled to a first approximation by two disordered triflate anions slightly separated along z and with their principal axes almost at right angles to each other. One is more highly occupied than the other, so that the oxygen atoms (disordered with and unresolvable from the corresponding fluorine atoms) are visible. The oxygen atoms in the other (low occupancy) ion interpenetrate with those of the first and so cannot be resolved. The carbon and sulfur atoms of each triflate are not resolvable and have been modelled by a sulfur atom with a nominal occupancy of 0.7, which was then refined to accommodate the distribution between the two perpendicular triflate anions (5:2). The highest peak in the final difference map (1.3 e/Å^3) appears next to this disordered anion.

$[Rh(12S3)_2](BF_4)_3$ gave systematic absence ($h0l$, l odd) uniquely consistent with space group $P2_1/c$. Fourier maps indicated that several ring C atoms were disordered. Normal anisotropic refinement gave large anisotropies for the temperature factors of both molecules in the asymmetric unit. In molecule 2 this effect was accompanied by anomalous values for some C–C and C–S bond lengths. Examination of a thermal ellipsoid plot for this molecule suggested that two segments of the ligand (C24, C21, C30, and C32) might be better represented by a disordered model with "half atoms" placed near each end of the major principal axis. This model was refined with similarity constraints on the C–S and C–C bond lengths and on the Rh–S–C, S–C–C, and C–C–C angles. The model was stable to refinement with isotropic temperature factors for the "split" atoms and gave an R factor essentially the same as for the normal anisotropic refinement. The similarity restraints were relaxed. Without performing an analysis at a different temperature it is not possible to say whether there is coordinated torsional libration about the Rh–S bonds or static disorder.

Results

Synthesis. Thioethers generally fail to displace halide ions from metal ions;[2] hence use of $RhCl_3 \cdot 3H_2O$ as a starting material necessitates the prior removal of Cl^- by reaction with silver triflate. Reflux of the resulting solution with a stoichiometric quantity of ligand yields $[Rh(L)_2]^{3+}$ (L = 9S3, 10S3, 12S3, ttn). This approach parallels the method used previously for preparation of analogous Ru(II) complexes[20] but without the concomitant reduction of the metal center that occurs with Ru(III).

Descriptions of the Structures. $[Rh(9S3)_2](CF_3SO_3)_3$ contains centrosymmetric $[Rh(9S3)_2]^{3+}$ cations in which coordination of two tridentate 9S3 units yields an octahedral RhS_6 coordination sphere (Figure 1). Two of the unique Rh–S distances (2.345 (3) Å and 2.348 (3) Å) are slightly longer than the third (2.331 (2) Å) (Table II). Interestingly, these distances (average 2.341 Å) just exceed those in the isoelectronic complex $[Ru(9S3)_2]^{2+}$ (Ru–S = 2.339 Å),[23,24] despite the increase in cationic charge. Intraligand dimensions and torsional angles differ negligibly from those found either in other complexes of 9S3[25] or, indeed, in the free

Table II. Selected Bond Lengths (Å) and Angles (deg) for $[Rh(9S3)_2](CF_3SO_3)_3$[a]

Rh–S1	2.331 (2)	Rh–S4	2.348 (3)
Rh–S7	2.345 (3)		
S1–C2	1.85 (1)	S1–C9	1.83 (1)
S4–C3	1.82 (1)	S4–C5	1.84 (1)
S7–C6	1.82 (1)	S7–C8	1.81 (1)
C2–C3	1.51 (2)	C5–C6	1.50 (2)
C8–C9	1.50 (2)		
S4–Rh–S1	88.5 (1)	S4–Rh–S1′	91.5 (1)
S7–Rh–S4	88.2 (1)	S7–Rh–S4′	91.8 (1)
S7–Rh–S1	89.0 (1)	S7–Rh–S1′	91.0 (1)

[a] Symmetry codes: (′) $^1/_2 - x, ^1/_2 - y, -z$; (″) $-x, y, ^1/_2 - z$.

Table III. Selected Bond Lengths (Å) and Angles (deg) for $[Rh(12S3)_2](BF_4)_2$[a]

Rh(1)–S(1)	2.360 (4)	S(29)–C(280)	1.78 (1)
Rh(1)–S(5)	2.356 (5)	S(29)–C(300)	1.79 (1)
Rh(1)–S(9)	2.361 (4)	S(29)–C(281)	1.79 (1)
Rh(2)–S(21)	2.345 (5)	S(29)–C(301)	1.79 (1)
Rh(2)–S(25)	2.344 (6)	C(2)–C(3)	1.43 (3)
Rh(2)–S(29)	2.353 (6)	C(3)–C(4)	1.45 (4)
S(1)–C(2)	1.83 (2)	C(6)–C(7)	1.48 (4)
S(1)–C(12)	1.82 (3)	C(7)–C(8)	1.52 (4)
S(5)–C(4)	1.84 (2)	C(10)–C(11)	1.45 (3)
S(5)–C(6)	1.82 (2)	C(11)–C(12)	1.33 (4)
S(9)–C(8)	1.82 (3)	C(23)–C(220)	1.54 (1)
S(9)–C(10)	1.84 (2)	C(23)–C(240)	1.54 (1)
S(21)–C(220)	1.79 (1)	C(23)–C(221)	1.53 (1)
S(21)–C(320)	1.78 (1)	C(23)–C(241)	1.53 (1)
S(21)–C(221)	1.78 (1)	C(27)–C(260)	1.54 (1)
S(21)–C(321)	1.78 (1)	C(27)–C(280)	1.54 (1)
S(25)–C(240)	1.79 (1)	C(27)–C(261)	1.53 (1)
S(25)–C(260)	1.78 (1)	C(27)–C(181)	1.55 (1)
S(25)–C(241)	1.79 (1)	C(31)–C(300)	1.55 (1)
S(25)–C(261)	1.78 (1)	C(31)–C(320)	1.55 (1)
		C(31)–C(301)	1.54 (1)
		C(31)–C(321)	1.54 (1)
S(5)–Rh(1)–S(1)	95.7 (2)	S(25)–Rh(2)–S(21)	93.4 (2)
S(9)–Rh(1)–S(1)	94.8 (2)	S(29)–Rh(2)–S(21)	94.7 (3)
S(9)–Rh(1)–S(5)	96.9 (2)	S(29)–Rh(2)–S(25)	94.7 (3)

[a] Symmetry codes: (′) $-x, -y, -z$; (:) $1 - x, -y, 1 - z$. Atoms in molecule are numbered S1, C2, C3, etc.; atoms in molecule 2 are numbered S21, C22, C23, etc. Three digit numbers represent atoms of partial occupancy related by disorder; hence C(220) and C(221) represent the two partially occupied positions that would be associated with C(22), if it were ordered.

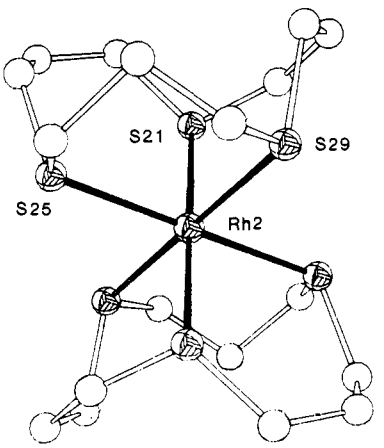

Figure 2. ORTEP diagram of $[Rh(12S3)_2]^{3+}$ (molecule 2), showing thermal ellipsoids at the 40% probability level. Atomic numbering analogous to Figure 1 (i.e., S21, C22, C23, etc.).

(23) Rawle, S. C.; Cooper, S. R. *J. Chem. Soc., Chem. Commun.* **1987**, 308.

(24) Bell, M. N.; Blake, A. J.; Schröder, M.; Küppers, H.-J.; Wieghardt, K. *Angew. Chem., Int. Ed. Engl.* **1987**, *26*, 250.

(25) Setzer, W. N.; Ogle, C. A.; Wilson, G. S.; Glass, R. S. *Inorg. Chem.* **1983**, *22*, 266.

Table IV. Redox Potentials (E vs SCE) and K_{disp} for $[Rh(L)_2]^{n+}$ Complexes

ligand	E(Rh(III/II)	E(Rh(II/I)	log K_{disp}
9S3	−309	−721	6.9
10S3	−246	−653	6.9
12S3	−125	−485	6.0

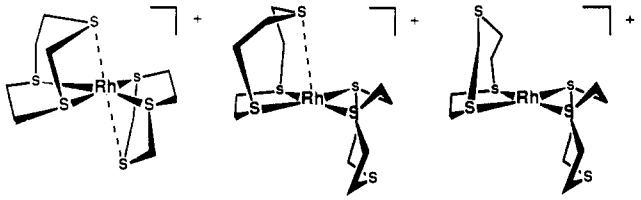

Figure 3. Possible geometries for $[Rh(9S3)_2]^+$ (see text).

ligand itself.[26] As pointed out previously,[2,3] 9S3 complexes owe their considerable stability in part to the excellent conformational match between free and bound ligand.

$[Rh(12S3)_2](BF_4)_3$ crystallizes with two crystallographically distinct but negligibly different $[Rh(12S3)_2]^{3+}$ cations in the unit cell. In each case, a Rh(III) ion interacts with six S atoms from the two 12S3 rings (Figure 2). Comparison with the 9S3 analogue reveals both dilation of the coordination sphere (Rh–S_{av} 2.356 Å, Table III; cf. 2.342 Å in $[Rh(9S3)_2]^{3+}$, Table II)[27] and expansion of the S–Rh–S chelate angles (∠S–Rh–S_{av} 95.8° and 85.6, respectively). Disorder of the 12S3 backbone prevents meaningful discussion of the ligand conformation.

Electrochemistry. Cyclic voltammetry in $MeNO_2$ on a glassy carbon electrode shows *two reduction processes* (Table IV), the first of which corresponds to a rare example of a monomeric Rh(II) complex.[28] Controlled potential electrolysis at −500 mV affords a straw-colored solution that exhibits a structureless EPR spectrum (at 298 K) with $g = 2.046$ (line width = 40 G). At 77 K frozen solutions given rhombic spectra with $g_1 = 2.085$, $g_2 = 2.042$, and $g_3 = 2.009$, with ^{103}Rh hyperfine splitting on g_1 (A-(^{103}Rh = 12 × 10^{-4} cm^{-1}; ^{103}Rh $I = {}^1/_2$ 100%). As in the isoelectronic complex $[Co(9S3)_2]^{2+}$, this g value pattern ($g_1, g_2 > 2$; $g_3 \approx 2$) is consistent with Jahn–Teller axial elongation of a d^7 ion to result in a d_{z^2} ground state (cf. the isoelectronic $[Pd(9S3)_2]^{3+}$ cation).[29] Analogous complexes of 10S3 and 12S3 show similar electrochemical behavior (Table IV) with progressively less reversibility; that of ttn fails to reveal any remotely well-behaved redox processes.

Discussion

Examples of likely geometries for $[Rh(9S3)_2]^+$ come from other platinum metal complexes of crown thioethers (Figure 3). In $[Pd(9S3)_2]^{2+}$ an essentially square-planar coordination sphere (Pd–$S_{eq,av}$ = 2.32 Å) interacts weakly with an axial thioether group (Pd–S_{ax} = 2.95 Å).[30] On the other hand, the square-pyramidal $[Pt(9S3)_2]^{2+}$ cation has four short Pt–S bonds (ranging from 2.25 to 2.30 Å) in the basal plane and a weak interaction with an apical thioether group (Pt–S = 2.91 Å); the remaining donor atom remains free.[30] Similar weak axial interactions occur in $[Pd(9S3)Br_2]$[31] and $[Pt(((MeO)_2benzo)_39S3)Cl_2]$.[32] In $[Rh(14S4)]_2Cl_2$·MeCN two square-planar RhS_4 units stacked face-to-face slip so that an S atom bound equatorially to one Rh can bind weakly (Rh–S_{ax} 3.70 to 3.82 Å) to the apical site of the other.[4] On balance square-pyramidal geometry appears more likely for $[Rh(9S3)_2]^+$. Comparison with the isoelectronic $[Pd(9S3)_2]^{2+}$ cation suggests that rhodium(I), owing to its smaller cationic charge, must engage in only the weakest axial interactions.

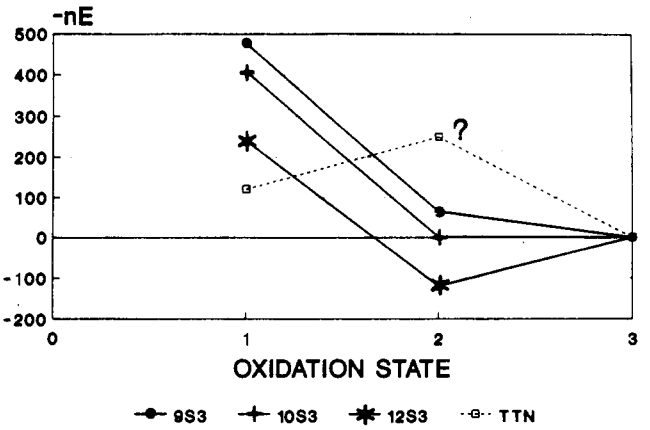

Figure 4. Oxidation state diagram for $[Rh(L)_2]^{n+}$ complexes (L = 9S3, 10S3, 12S3, ttn) (see text).

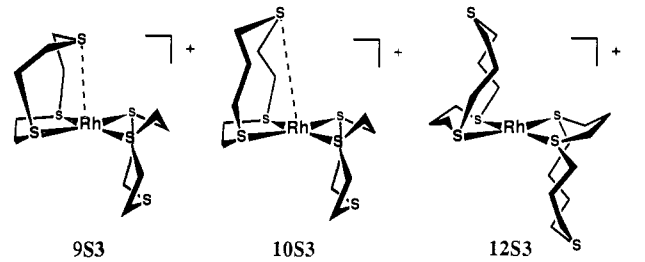

Figure 5. Schematic representation of progressively weaker imposition of six-coordination on $[Rh(L)_2]^+$ as ring size increases from L = 9S3 (left) to 12S3 (right); L = ttn (far right).

Both thermodynamic and kinetic factors contribute to the observation of monomeric Rh(II) species in this system. The thermodynamic stability of $[Rh(9S3)_2]^{2+}$ with respect to disproportionation (Table IV) derives from both the electronic and steric properties of this crown thioether. Thioethers stabilize low oxidation states through their appreciable π-acidity and their poor ability to neutralize positive charge (owing to their low σ-donor ability).[2] Hence electronically 9S3 destabilizes Rh(III) with respect to (II) and (I). On the other hand, incorporation of three thioether donors into a ring tends to enforce 3- or 6-fold coordination (for mono or bis complexes, respectively). Consequently 9S3 disfavors 4-fold coordination; it therefore destabilizes Rh(I) with respect to (II) and (III). Imposition of five- or six-coordination on Rh(I) destabilizes it stereochemically with respect to the six-coordinate Rh(III) complex. Crown thioethers set in apposition to these cross-cutting electronic and stereochemical effects and thereby disfavor *both* Rh(III) *and* Rh(I) with respect to Rh(II). Thus the existence of $[Rh(9S3)_2]^{2+}$ results from *destabilization* of Rh(III) and Rh(I) through the electronic and stereochemical properties of the ligand, respectively.

A plot of $\Delta G_{formation}$ versus oxidation state (i.e., an oxidation state diagram[33] (Figure 4) clarifies the role of conformation in controlling the tendency toward disproportionation. (In the absence of absolute thermodynamic values, $\Delta G_{formation}$ of the Rh(III) complexes has arbitrarily been taken as zero to facilitate comparison of the curves.) For each ligand interest focuses on (1) the convexity or concavity of the curve and (2) the slope of the line connecting the points corresponding to Rh(III) and Rh(I). The more concave the plot (i.e., the further the point for Rh(II)

(26) Glass, R. S.; Wilson, G. S.; Setzer, W. N. *J. Am. Chem. Soc.* **1980**, *102*, 5068.

(27) The dilation in this case (0.015 Å) is less than half that in the Ru(II) complexes. This may reflect a "harder" Rh–S force constant.

(28) For rare examples of monomeric Rh(II) complexes, see: Bennett, M. A.; Bramley, R.; Longstaff, P. A. *J. Chem. Soc., Chem. Commun.* **1966**, 806. Dunbar, K. R.; Haefner, S. C.; Pence, L. E. *J. Am. Chem. Soc.* **1989**, *111*, 5504.

(29) Blake, A. J.; Holder, A. J.; Hyde, T. I.; Schröder, M. *J. Chem. Soc., Chem. Commun.* **1987**, 987.

(30) Blake, A. J.; Holder, A. J.; Hyde, T. I.; Roberts, Y. V.; Lavery, A. J.; Schröder, M. *J. Organomet. Chem.* **1987**, *323*, 261.

(31) Wieghardt, K.; Küppers, H.-J.; Raabe, E.; Krüger, C. *Angew. Chem., Int. Ed. Engl.* **1986**, *25*, 1101.

(32) Von Deuten, K.; Klar, G. *Cryst. Struct. Commun.* **1981**, *10*, 757.

(33) *Inorganic Chemistry*; Phillips, C. S. G., Williams, R. J. P., Eds.; Oxford University Press: 1965; Vol. I, p 314.

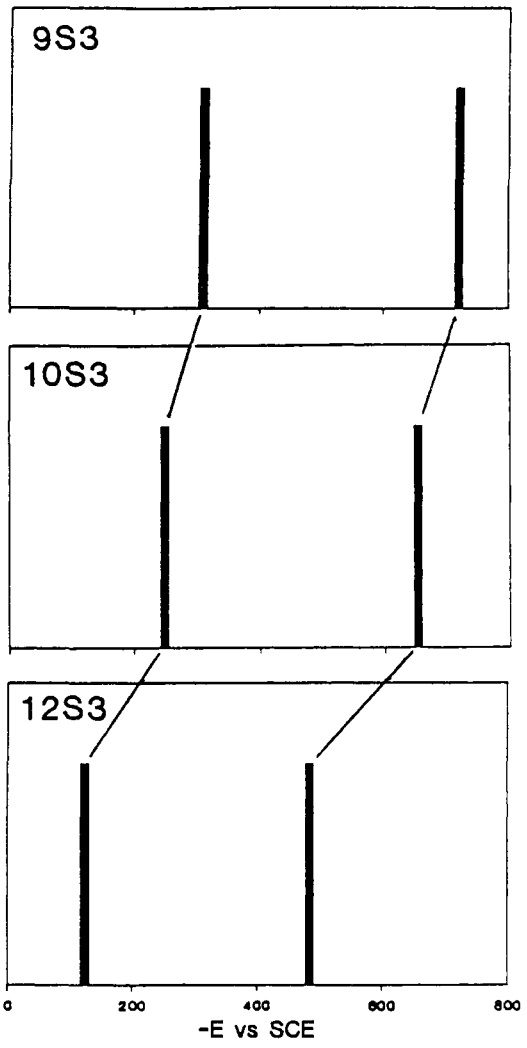

Figure 6. Reduction potentials of $[Rh(L)_2]^{n+}$ complexex (L = 9S3, 10S3, 12S3).

lies below the line connecting Rh(III) with Rh(I)) the greater the thermodynamic stability of Rh(II) with respect to disproportionation.

Across the series $[Rh(L)_2]^{n+}$ (L = 9S3, 10S3, 12S3, ttn) relaxation of the conformationally imposed six-coordination (Figure 5) progressively diminishes the stability of Rh(II) with respect to disproportionation (as shown by the decreasing convexity of the plot) (Figure 4). It also stabilizes Rh(I) with respect to Rh(III), as shown by the diminishing slope of the line connecting these two oxidation states. Removal of all conformational constraint (L = ttn) moves $[Rh(L)_2]^{2+}$ *above* the line connecting the flanking oxidation states. Accordingly, in this case Rh(II) disproportionates, as most Rh(II) do. The instability of $[Rh(L)_2]^{2+}$ for L = ttn establishes that its stability for L = 9S3, 10S3, and 12S3 does not arise simply from thioether coordination. Rather, the contrast emphasizes the role of ligand conformation in controlling the solution chemistry.

Across the series $[Rh(L)_2]^{3+}$ (L = 9S3, 10S3, 12S3) both the Rh(III/II) and Rh(II/I) potentials shift to more positive values (Figure 6, Table IV). On a simplistic level one would expect larger ring ligands to favor lower oxidation states, since reduction increases the ionic radius of a metal ion. Addition of a methylene group increases the Rh(III/II) potential on average by ca. 60 mV. Similarly, it increases the Rh(II/I) potential by ca. 80 mV on average. From $E_{complex} - E_0 = (RT/nF) \ln \{K_{ox}/K_{ref}\}$ each methylene group therefore destabilizes Rh(III) (with respect to Rh(II)) by approximately 10-fold in equilibrium constant (i.e., 1.3 kcal/mol). Each destabilizes Rh(II) with respect to Rh(I) slightly more (approximately 20-fold; 1.7 kcal/mol). Compared to 9S3 the larger rings need to pay less conformational cost in adapting to the stereochemistry of Rh(I).

Comparison of the *difference* between Rh(III/II) and Rh(II/I) potentials shows the effect of ring size on K_{disp}, the equilibrium constant for disproportionation (Figure 6, Table IV). This difference remains nearly constant at ca. 410 mV on going from 9S3 to 10S3 ($K_{disp} = 10^{-7}$). This result probably means that the primary interaction between 10S3 and Rh(III/II/I) occurs through ethyl-linked S atoms, which are common to both ligands. For the 12S3 complex, however, which has only propyl-linked S atoms, ΔE decreases to 360 mV ($K_{disp} = 10^{-6}$). Thus coordination through propyl-linked S atoms increases the tendency of Rh(II) to disproportionate, largely by stabilizing Rh(I).

Besides these thermodynamic factors, the crown thioethers also favor the existence of Rh(II) species kinetically. By hindering access to the metal center they inhibit dimerization (as occurs in, e.g., $[Rh(14S4)]^{2+}$ to give $[RhCl(14S4)]_2^{2+}$).[4] Electrochemically generated solutions of $[Rh(9S3)_2]^{2+}$ maintain their electrochemical response for over an hour. Like the thermodynamic effect described above, this kinetic stabilization presumably reflects the unusual conformational properties of 9S3 (and to a much less extent, 10S3 and 12S3). Owing to following chemical reactions electrochemical reversibility progressively decreases with increasing ring size, while the acyclic complex $[Rh(ttn)_2]^{3+}$ shows no reversible electrochemistry at all.

Conclusions

The remarkable stabilization of Rh(II) by 9S3 appears to arise predominantly from the conformational constraints of the ligand, not from the mere presence of a hexakis(thioether) coordination sphere. By extension other 9S3 complexes in unusual oxidation states presumably owe their existence, at least in part, to the unique conformational properties of the ligand.

Acknowledgment. We are grateful to the Petroleum Research Fund, administered by the American Chemical Society, for support of this researh.

Registry No. $[Rh(9S3)_2](CF_3SO_3)_3$, 110294-65-0; $[Rh(10S3)_2](BF_4)_3$, 131617-57-7; $[Rh(12S3)_2](BF_4)_3$, 131617-59-9; $[Rh(ttn)_2](BF_4)_3$, 131617-61-3; $[Rh(9S3)_2]^{2+}$, 110294-66-1; $[Rh(10S3)_2]^{2+}$, 131617-62-4; $[Rh(12S3)_2]^{2+}$, 131617-63-5.

Supplementary Material Available: Listings of crystallographic data, bond lengths and angles, anisotropic thermal parameters, hydrogen atom positional and thermal parameters, and atomic coordinates and thermal parameters for $[Rh(9S3)_2](CF_3SO_3)_3$ and $[Rh(12S3)_2](BF_4)_3$ (12 pages); listings of observed and calculated structure factors (26 pages). Ordering information is given on any current masthead page.